High Resolution Dual Material Stereolithography for Monolithic Microdevices

Schmidleithner, Christina; Zhang, Rujing; Taebnia, Nayere; Larsen, Esben K. U.; Almdal, Kristoffer; Larsen, Niels B.

Published in:
Advanced Materials Technology

Link to article, DOI:
10.1002/admt.202101180

Publication date:
2022

Document Version
Peer reviewed version

High Resolution Dual Material Stereolithography for Monolithic Microdevices

*Christina Schmidleithner, Rujing Zhang, Nayere Taebnia, Esben K. U. Larsen, Kristoffer Almdal, Niels B. Larsen**

C. Schmidleithner, Dr. R. Zhang, N. Taebnia, Prof. N. B. Larsen
Dept. of Health Technology, DTU Health Tech, Technical University of Denmark,
Ørsteds Plads 345C, 2800 Kgs. Lyngby, Denmark
E-mail: nibl@dtu.dk

Dr. E. K. U. Larsen[+], Prof. K. Almdal
Dept. of Chemistry, Technical University of Denmark,
Kemitorvet 206, 2800 Kgs. Lyngby, Denmark

[+] Current address: Coloplast A/S, Holtedam 1, 3050 Humlebæk, Denmark

Keywords: dual material stereolithography, hydrogels, additive manufacturing, monolithic devices, advanced cell culture, 3D printing

Functional 3D components such as perfusion channels and mechanical actuation elements at cellular length scales can support cell survival and tissue maturation in tissue modeling devices. These advanced requirements call for increasingly complex materials and 3D fabrication methods. Here, a high-resolution dual-material 3D printing concept is developed, where distinct materials are produced locally by orthogonal chemical reactions depending on the illumination wavelength. A tough, stiff epoxy network results from cationic polymerization in UV light, while a soft and diffusion-open hydrogel forms by free-radical polymerization initiated by blue light. Thus, dual-exposure allows for selection of material properties in every voxel, while retaining the 3D design flexibility associated with stereolithography. This enables single-process fabrication of devices integrating mechanically stable chip-to-world interconnects and compliant, diffusion-open perfusable channel components of 150 μm in width and height, while also allowing structural and mechanical feature dimensions down to 60 μm. A perfusion chip capable of creating a stable uni-axial chemical gradient by passive dye diffusion through hydrogel sections, and a negative Poisson ratio structure based on the interplay between stiff rotators and compliant hinges, are

manufactured as proof of concept microdevices. Lastly, week-long culture of hydrogel-encapsulated human liver cells demonstrates the cytocompatibility of both materials.

1. Introduction

Compliant hydrogels can support diffusive nutrient supply and waste removal to and from cells due to their highly swollen network structure. These properties make hydrogels attractive materials for tissue modeling applications.[1,2] Models should ideally mimic the *in vivo* cellular microenvironment through precise engineering of fluid flow in combination with control of chemical, physical, and mechanical cues.[3] The incorporation of structured hydrogels in existing microfluidic devices has been investigated extensively.[4,5] However, conventional soft lithography approaches for the assembly of these systems consist of multi-step procedures and lack design flexibility. 3D printing methods would be suitable as single-step and highly adaptive fabrication alternatives.[6–10] The present manuscript describes a dual material stereolithography (SLA) system to combine high resolution and design flexibility with the possibility of spatial hydrogel material selection in a monolithic format.

Spatial control of water-soluble chemical signals is attainable by combining diffusion-open and diffusion-closed segments. Free diffusion of soluble components in the hydrogel environment can be further exploited in the generation of chemical gradients.[11,12] Combining a soft hydrogel with a stiffer material enables formation of spatially controlled biophysical cues, that can simulate physiological conditions.[13,14] Integration of moving parts, for instance for mechanical stimulation of tissue constructs, requires that the secondary material has sufficient toughness to withstand the actuator stroke. Toughness is also a vital factor for the creation of stable chip-to-world interconnects, sustaining the external forces applied during connection and de-connection. Stable adhesion at internal interfaces of the primary and secondary materials is equally important for producing robust devices, ideally forming continuous, monolithic entities. In addition to the bulk material properties, material shaping in

3D at cellular length scales is required. Lastly, the ability to integrate channel microstructures for oxygen and nutrient transport by advective flow is essential for the survival of 3D cultures at high cell densities.[15]

SLA is a suitable candidate for the required materials shaping, given its routinely achievable feature size of <100 µm and high volumetric throughput. A major disadvantage of SLA, in contrast to extrusion-based 3D printing,[16–18] is its general restriction to printing one material at a time. SLA printing with multiple materials has formerly been achieved by physical switching between resin baths and complex washing steps during printing.[19–21] Recently, more rapid resin switching was achieved by dynamic fluidic control.[22,23] Modification of material properties without exchange of resin has been explored by grayscale illumination[24–26] or varying post-curing parameters.[27] Dolinski *et al.* reported on a dual material SLA system using photo-bleachable molecules. Depending on the wavelength, either a radical or a cationic reaction is initiated and manufacturing of a single-layered volumetric object from two different materials is possible in a single resin bath.[28] Schwartz and Boydston also used independent initiation of a radical and a cationic reaction in a process true to the 3D printing concept, as structures consisting of multiple layers can be created.[29] However, their reported spatial resolution was in the range of centimeters, which is insufficient for local composition control at cellular length scales.

This work employs digital light processing (DLP) based SLA to manufacture two distinct materials for advanced cell culture applications. The material system (**Figure 1**a) consists of a radical curing reaction initiated by blue light and an independent cationic component polymerized only in UV, a concept described in our former publication.[30] The free radical reaction leads to formation of a pure poly(ethylene glycol) diacrylate (PEGDA) hydrogel, a highly swelling and compliant material, open to diffusion of aqueous substances. The ring

opening cationic reaction of 3,4-Epoxycyclohexylmethyl-3',4'-epoxycyclohexane carboxylate (EEC) creates an interpenetrating network of EEC and PEGDA, a stiffer, diffusion-closed material. Printing proceeds by generation of two distinct STL files from the computer-aided design (CAD), one for each material, and their slicing into the desired layer thickness, here 20 µm. In each printed layer, the curing pattern for either material is then projected sequentially in UV or blue light, thus generating a 3D object with a choice in material possible for every voxel (Figure 1b).

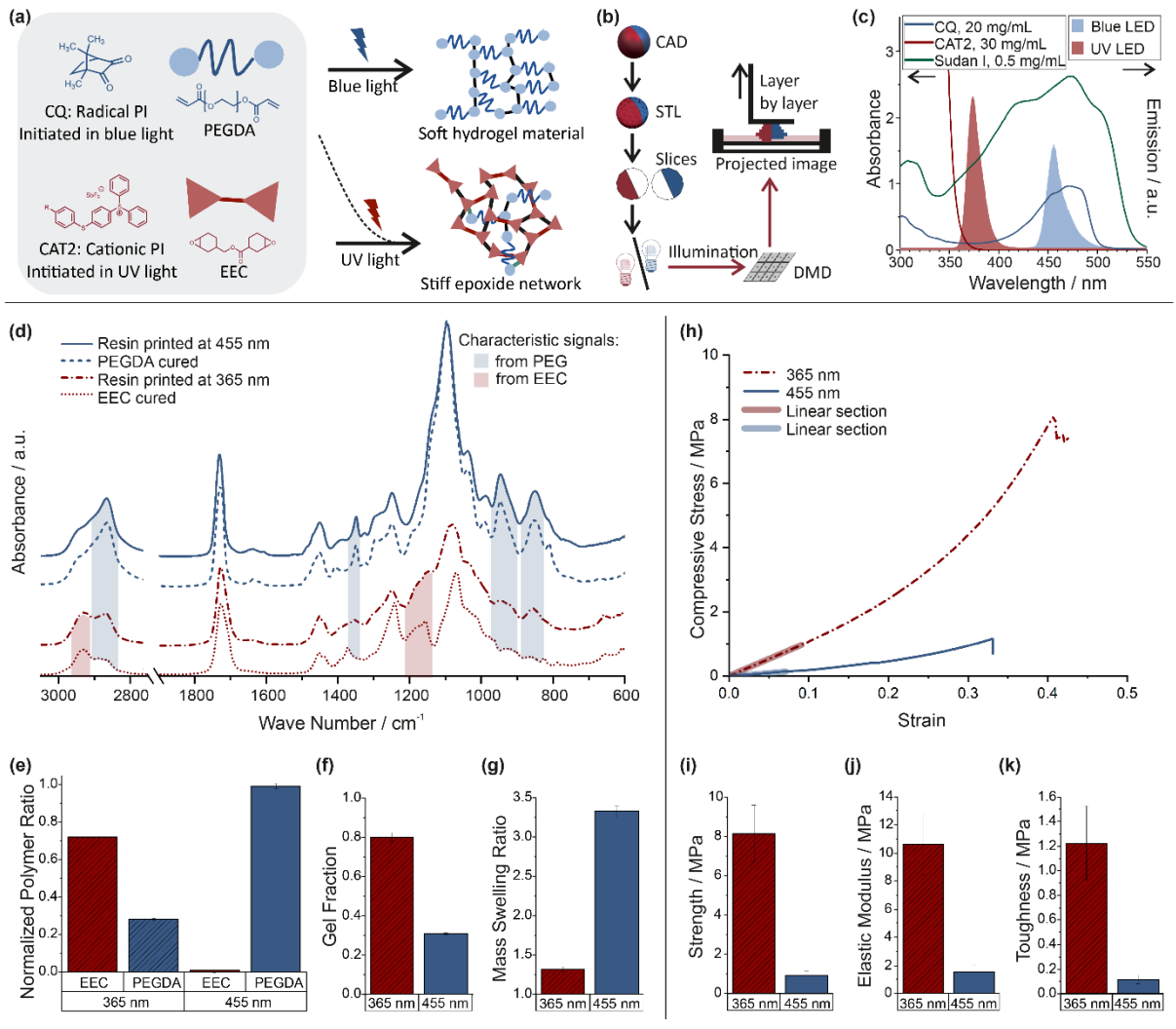

Figure 1. (a) Reaction scheme for the radical polymerization of PEGDA (blue) and the cationic polymerization of EEC (red), triggered by blue or UV light, leading to the formation of two different polymer networks. (b) Overview of the dual material SLA process. (c) UV-Vis absorption (2 mm light path) of photoinitiators (CQ and CAT2) and absorber (Sudan I). Emission spectra of the blue and UV LEDs are overlaid. (d) ATR FT-IR spectra of individually cured monomers and of the resin printed at 455 nm or 365 nm. Blue shaded peaks are PEGDA specific signals present in materials printed at either wavelength. Red

shaded peaks are from EEC only present after printing at 365 nm. (e) Normalized polymer ratios in printed parts determined from fitting of the components' spectra to the ATR-FTIR measurements. (f) Gravimetric gel fraction of printed parts determined by Soxhlet extraction in dichloromethane (n = 5). (g) Gravimetric swelling ratio of printed parts (n = 5). (h) Compression testing of Ø5 mm x 5 mm cylindrical structures, swollen in water. (i) Compressive strength obtained from maximum nominal stress. (j) Elastic modulus calculated from the linear section in the stress-strain curves. (k) Toughness calculated from area under the stress-strain curves (n = 9). Error bars show the standard deviation.

2. Results and Discussion

Multiple factors need to be considered in the development of a 3D printing resin relying on orthogonal chemistries to polymerize two different materials, specifically free radical versus cationic initiation. The first factor is selectivity. Here, selective radical initiated polymerization is attained by choosing a cationic initiator incapable of being activated by free radicals. Triarylsulfonium hexafluoroantimonate salt (CAT2) is used as the cationic photoinitiator (PI). Upon illumination in the UV range, creation of cations and radicals initiates both relevant reactions.[31] Contrary to diaryliodonium salts, which are often employed in initiator systems for radical and cationic hybrid polymerizations,[32–34] CAT2 cannot be activated by free radicals, due to its high reduction potential.[31] This eliminates unwanted epoxide curing during illumination at 455 nm. The type II radical PI camphorquinone (CQ) with its co-initiator ethyl 4-dimethylaminobenzoate (EDMAB) exclusively initiates radical polymerization when exposed to blue light,[35] thus generating the PEGDA hydrogel. The second factor is fast light-induced solidification. Each layer is cured in succession, so the exposure time needed for sufficient conversion at either wavelength must be minimized to reduce printing time. The third factor is adequate lateral printing resolution, as polymerization should ideally be restricted to the illuminated cross-section. The last factor is that the layer cure depth must be limited for vertical feature development while still allowing for sufficient layer-to-layer adhesion.[36] For details of development of the resin for high-resolution printing, see the Supporting Information and Figure S1-S5. At an exposure time of 10 s at either 365 nm or 455 nm, both developed systems exhibit a cure depth of just

above 100 µm (Figure S5), supporting the selection of this printing time per 20 µm layer. This excessive cure depth is beneficial for robust printing, as stable layer-to-layer adhesion is required during the printing process, and as cure depth does not necessarily reflect conversion or stability of the formed gel,[37] but comes at a cost of limited vertical resolution.

The material composition of printed structures was investigated by curve fitting of component IR spectra to print spectra (Figure 1d). The material printed at 455 nm corresponds to that of pure, polymerized PEGDA, while the material printed at 365 nm shows signals both of cured PEGDA (28%) and of polymerized EEC (72%) (Figure 1e). Thus, formation of two distinct materials is confirmed. Gel fractions are shown in Figure 1f and the difference in aqueous swelling capabilities (Figure 1g) is essential for printing of devices with diffusion-open and diffusion-closed segments. Mechanical properties of the two printed materials were evaluated by compression testing, with representative stress-strain curves shown in Figure 1h. The printed epoxy network is stronger (Figure 1i), stiffer (Figure 1j), and tougher (Figure 1k), than the PEGDA hydrogel. For mechanical analysis according to the neo-Hookean model for hyperelastic materials, see Figure S6.

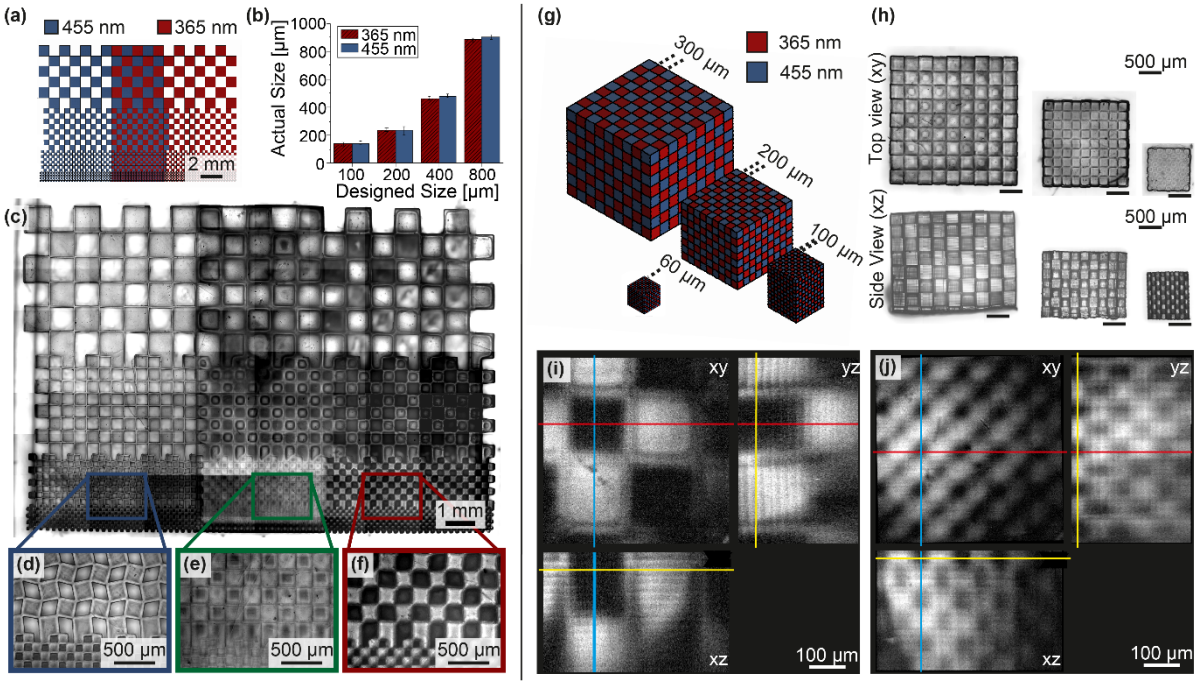

Figure 2. Printed structures for analysis of feature development and resolution. (a-f) Vertically extruded 2D checkerboard structure printed to a height of 1 mm. (a) Top-view of the print design. (b) Measured (microscopy) checkerboard side lengths versus design size (n = 3). Error bars show the standard deviation. (c-f) Representative reflected light micrograph of the print submerged in water. Vacancies appear bright in the PEGDA part (d) and dark in the epoxy part (f). Pure PEGDA appears bright in the mixed PEGDA/epoxy part (e). (g-j) 3D checkerboard structures with alternating EEC or PEGDA cubes of 60-300 µm side lengths. (g) Print design. (h) Top- and side-view reflected light micrographs of 100-300 µm cubes submerged in water (side view samples cut from their glass support). (i-j) Two-photon microscopy of a 200 µm and a 60 µm checkered structure (brighter cubes PEGDA; darker cubes EEC).

Checkerboard patterns of alternating filled or void spaces and of alternating materials were printed to assess achievable design fidelity (**Figure 2**a-f). Printing in both materials shows a tendency to produce slightly enlarged structures (Figure 2b). This could be due to lateral over-polymerization, especially for the smaller features, or due to excessive swelling for the larger cubes. Material selectivity in all three dimensions was investigated by printing 3D checkerboard structures with a design of alternating EEC and PEGDA cubes (Figure 2g-j). Distinct cubes are clearly visible on the surface of the printed structures (Figure 2h). Two-photon microscopy shows well defined material selection also within the prints (Figure 2i-j). The individual printing layers of 20 µm are discernible from the intensity gradient of PEGDA-related auto-fluorescence within each layer. As in all SLA processes, the irradiation intensity decreases exponentially according to Beer-Lambert's law when progressing further into each printed layer.[36] This leads to a gradient of initiation within the layers,[38] visualized by auto-fluorescence of the radical co-initiator EDMAB in our system. The three individual layers forming each cube in the 60 µm checkered structure and the alternation of EEC and PEGDA units are clearly visible, even on this small scale.

Printing of perfusable channels is essential in many devices employed in tissue models. As discussed, a cure depth of approximately 100 µm is expected for either material at 10 s illumination. Two photon microscopy (**Figure 3**a-g) shows that 200 µm channels were

polymerized shut when printing at either wavelength with standard printing conditions. The excessive over-curing suggests that the uncured material in the channel volume receives illumination from multiple layers exposed after the channel ceiling layer,[39] leading to polymerization in the designed void space (see Supporting Information and Figure S7-S11).

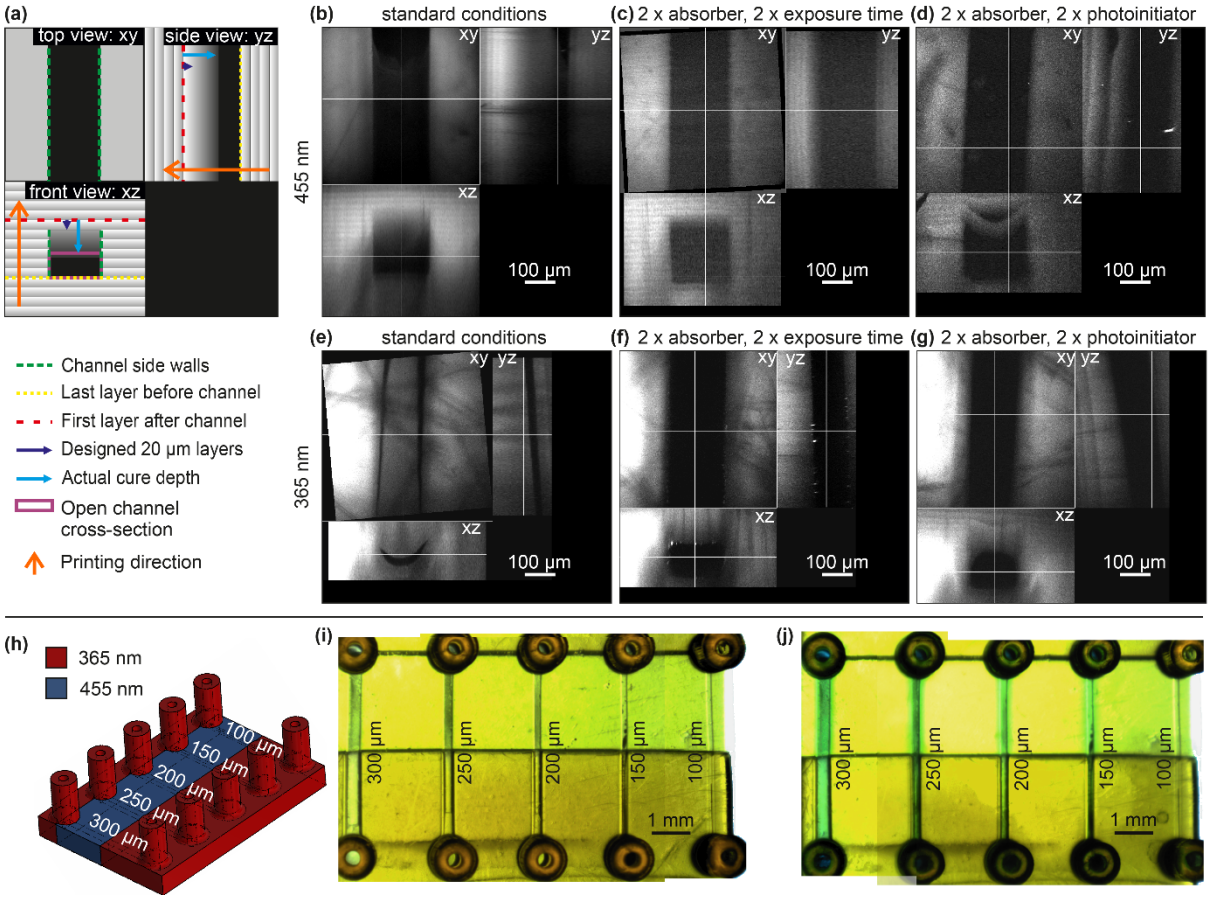

Figure 3. (a) Illustration of channels visualized by two-photon microscopy showing individual layers, their cross-linking gradients, and over-curing into the designed void space. (b-g) Two photon microscopy of 200 x 200 µm^2 closed square channels printed using 455 nm or 365 nm light with 10 µg mL^{-1} acrylate functionalized Rhodamine B, post-cured, and swollen in water. (b and e) Printed in 'standard conditions' (1.5 mg mL^{-1} Sudan I absorber, 10 s exposure). (c and f) Printed in '2 x absorber, 2 x exposure time' conditions (3 mg mL^{-1} Sudan I, 20 s). (d and g) Printed in '2 x absorber, 2 x photoinitiator' conditions (3 mg mL^{-1} Sudan I, 10 s, 60 mg mL^{-1} CAT2, 40 mg mL^{-1} CQ). (h-j) Perfusable channels printed using optimized conditions (3 mg mL^{-1} Sudan I, 20 mg mL^{-1} CQ, 60 mg mL^{-1} CAT2, 10 s at 365 nm, 20 s at 455 nm). (h) Design of 100 – 300 µm channels. (i) Print before perfusion. (j) Print after perfusion with green dye. Channels ≥150 µm are perfusable and dye diffuses into PEGDA printed at 455 nm.

To limit penetration depth into the resin and to reduce over-curing, the absorber content in the resin was doubled. Simultaneously, either exposure time or PI content were doubled, to

compensate for the lower energy dose available for polymerization. Figure 3b-g shows that increasing the absorber concentration substantially decreases the vertical over-curing observed for the standard printing condition, leading to well defined channels especially with the longer exposure time parameter set. Cure depth seems further decreased when increasing PI concentrations instead of exposure time. This leads to inadequate layer adhesion and, particularly for PEGDA, can compromise the channels' structural integrity. Nevertheless, the positive effect of higher absorber concentration on the channel printability is evident as the channels become well defined (see Supporting Information and Figure S10+S11 for 60 – 300 µm channels). From these different printing conditions, the most favorable one for printing at 455 nm is the 2 x absorber and 2 x exposure time condition, as it leads to small patent channels with sufficient layer adhesion. For printing at 365 nm, however, the 2 x absorber and 2 x photoinitiator parameter is superior, as it achieves the smallest channels. A combination of the two conditions with 3 mg mL^{-1} Sudan I absorber, 20 mg mL^{-1} CQ, 60 mg mL^{-1} CAT2, 20 s exposure time at 455 nm and 10 s exposure time at 365 nm is thus selected as the optimized channel printing procedure used in the further work.

Chips with designed channel widths and heights of 100 – 300 µm were printed using the optimized conditions at 455 nm and 365 nm to show that printed channels are perfusable (Figure 3h-j). A green dye was pumped through and channels down to 150 µm were found patent. While dye diffuses into the printed PEGDA material, visible by blue coloring of the printed hydrogel in the channel vicinity, channel sections printed with EEC are diffusion closed.

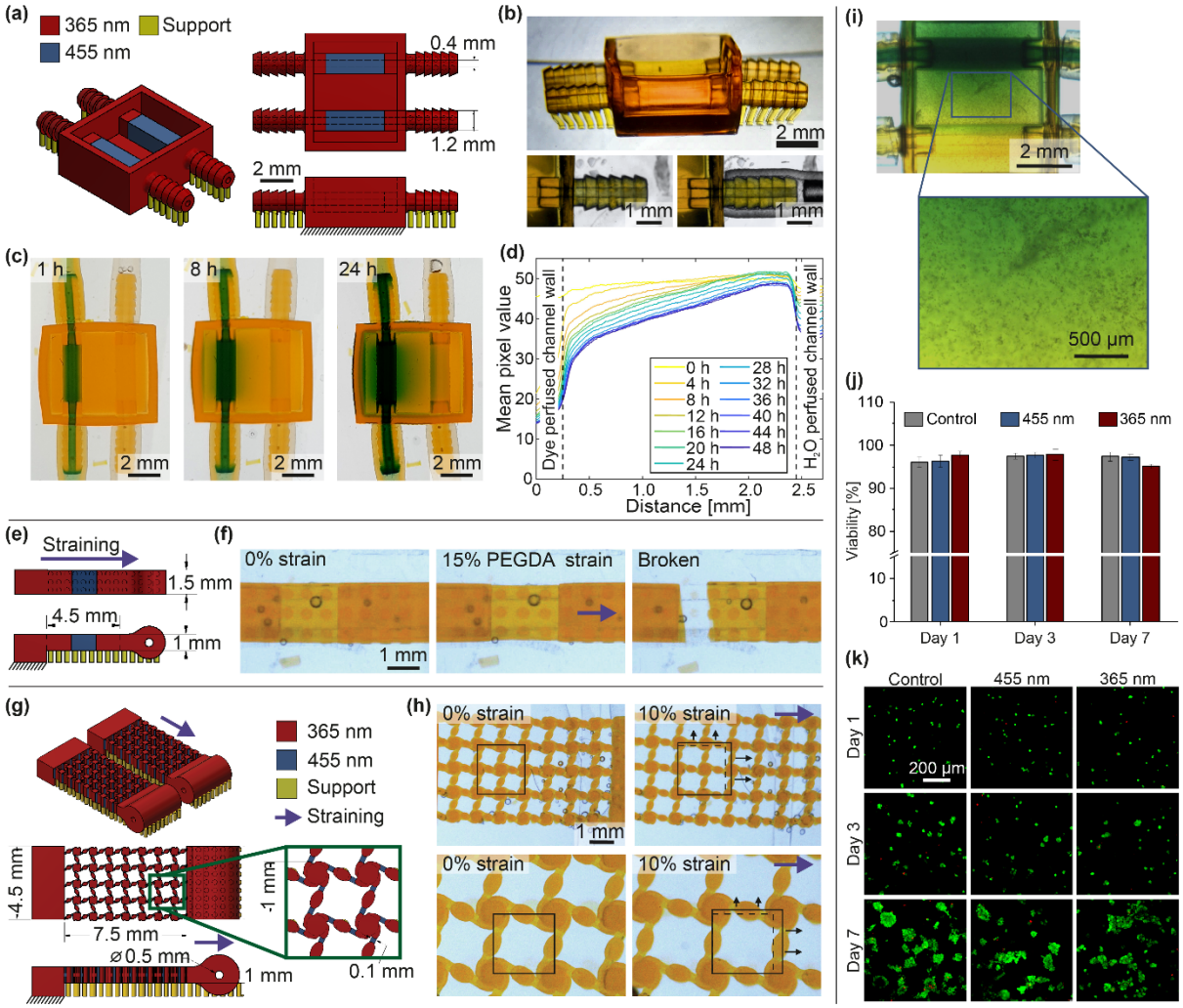

Figure 4. Monolithic devices printed using optimized conditions (see Fig. 3 caption). Yellow support structures were printed at 455 nm and removed after printing. (a-g) Generation of a stable chemical gradient. (a) Design of perfusion chip. (b) Photos of printed chip before perfusion with magnification of barbed tubing connectors. (c) Photos during perfusion. (d) Mean red pixel value as a function of distance between the channels plotted every 4 h showing creation of a stable chemical gradient after 24 h. (e-f) Investigation of material behavior under tension. (e) Design of the strainable structure with 0.5 mm hole for insertion of a needle and actuation. (f) Images of the printed structures submerged in water in unstrained, strained, and broken conditions, showing fracture through the PEGDA section. (g-h) Fabrication of a negative Poisson ratio structure adapted from [40]. (g) Design of the structure. (h) Images of unstrained and strained structures, submerged in water, with increase in dimensions in both directions upon strain. (i-k) Culturing of HepG2 cells encapsulated in Matrigel matrix in printed structures for 1 week. (i) Cells cultured in the chips described in (a-d) for 7 days with subsequent perfusion of the chip and creation of a dye gradient in the presence of cells. Images were taken while submerged in water, 24 h after start of perfusion. (j) Viability of cells cultured in wells printed at either 365 nm or 455 nm calculated as area of live cells over sum of the area occupied by dead and live cells. Controls were Matrigel-encapsulated HepG2 cultured in TCPS dishes (n = 4). No statistically significant difference was found between the different groups at any time-point as calculated by two-way ANOVA in GraphPad Prism. Error bars show the standard deviation. (k) Fluorescence micrographs of live (green)/dead (red)-stained encapsulated HepG2 cells after 1, 3, and 7 days of culture.

As a proof of concept, perfusion chips with integrated chip-to-tube connections and capable of generating a chemical gradient were printed (**Figure 4**a-d). Robust and reliable connections are often challenging to attain,[41] yet paramount to stable and reproducible perfusion; therefore, barbed tubing connectors were printed in the tougher epoxide material. Only the center channel sections, where diffusion of aqueous substances through the walls is desired, are printed at 455 nm to produce the PEGDA hydrogel. After 24 h of continuous perfusion of both channels, a stable dye gradient is observed (Figure 4d).

Behavior of the materials under tension and strength of their interfacial adhesion was investigated by controlled straining (see Figure S12 for the setup). When straining alternating sections of the PEGDA hydrogel and the epoxy network (Figure 4e+f), most of the deformation under tension occurs in the softer PEGDA areas, as expected from the mechanical compression analysis (Figure 1h-k). While PEGDA is strained by up to 15%, the epoxy sections only elongate by 2%. To exploit these material differences and demonstrate the possibility of combining stiff rotators and compliant hinges, a negative Poisson ratio structure was printed (Figure 4g+h). The design was adapted for printability from topology-optimized structures by Wang *et al.*[40] 10% strain in the actuation direction leads to 5% strain in the orthogonal direction, corresponding to a Poisson ratio of -0.5.

Lastly, the viability of HepG2 cells as a model cell line was evaluated to study the materials' cytocompatibility. 3D printed bowl-like wells (Figure S15) composed of the two different materials were used. After thorough washing, as also monitored in UV-VIS (Figure S13-S14), hydrogel-encapsulated cells were cultured (see Supporting Information for details), and their viability and proliferation were monitored for 7 days (Figure 4j-k). Cellular morphology and the results from live/dead staining indicate that all 3D printed structures support cell

proliferation (Figure S16) and do not elicit any cytotoxic effects. We observed a high viability (>90%) for both materials on day 1, which remains similar to cells cultured in 3D hydrogels in conventional tissue culture polystyrene (TCPS) well plates over the course of 7 days (Figure 4j+k).

3. Conclusions

The dual-material SLA process presented in this manuscript enables printing of two distinct materials from a single resin bath. Ten seconds exposure either in UV or in blue light can direct polymerization of an epoxide network or a PEGDA hydrogel in each voxel. Thus, printing speeds of 2.25 mm/h could be achieved for 20 µm layers, and perfusable channels in the size range of 150 µm were printed from both wavelengths. The utilized materials exhibit distinct swelling behavior, differ in mechanical properties, and are generated from individual chemical reactions. This allows for additional dimensions in design flexibility associated with additive manufacturing processes. We have shown that the large difference in water swelling can be exploited by printing diffusion-open and diffusion-closed features within one design. The 7-fold change in stiffness and 10-fold difference in toughness enables fabrication of stable tubing connectors and mechanical anchor points, while retaining the possibility of including more compliant diffusion-open hydrogel sections within one print. Interfacial adhesion between the two materials was shown to be sufficient, also under tension, for creation of strainable negative Poisson ratio structures. Finally, in a 7-day cell culture experiment, we find both materials to show equal cytocompatibility to cultures in standard well plates. The foundation for a robust dual material SLA system has been laid in the present manuscript, which could facilitate fast and simple manufacturing of a variety of multi-functional tissue modeling devices.

4. Experimental Section

The custom-built stereolithographic printer has been previously described.[42] The DMD has a pixel pitch of 10.8 µm and the two utilized LEDs at 365 nm and 455 nm yield power densities at the vat bottom of 10.9 mW cm^{-2} and 22.0 mW cm^{-2}, respectively. Methacrylate-silane treated cover-glasses was used as build-supports to ensure adhesion of the printed part.[41] Autodesk Inventor Professional 2018 (Autodesk) was applied to generate CADs as well as the corresponding STL files, and the open-source software Slice3r was employed for slicing into printing layers. All chemicals were purchased from Sigma Aldrich, except for the hetero-bifunctional crosslinker 3-ethyl-3-(acryloyloxy)methyloxetane (OXA-acrylate) synthesized (Supporting information) according to a published method.[43] Unless stated otherwise, the following resin composition is used and referred to as the standard formulation (Sigma Aldrich item number in brackets): EEC (407208; 50% v/v), PEGDA (455008; 30% v/v), CAT2 (654027; 30 mg mL^{-1}), CQ (124893; 20 mg mL^{-1}), Sudan I (103624; 1.5 mg mL^{-1}), EDMAB (E24905; 0.1 eq. to CQ, 2.3 mg mL^{-1}), 1,2-propanediol (398039; 0.25 eq. to EEC, 44 mg mL^{-1}), and OXA-acrylate (0.05 eq. to EEC, 20 mg mL^{-1}) with 20 µL mL^{-1} diethylene glycol diethyl ether (DGDE; 8.02932) and 30 µL mL^{-1} propylene carbonate (PC; 8.07051) as solvents. For each print, at least 1.5 mL of the resin solution is added to the transparent printer vat. Each 20 µm layer is exposed for 10 s at 365 and/or 455 nm. The first four layers were reduced to 10 µm thicknes to ensure sufficient adhesion to the cover-glass. After printing, samples were post-cured thermally in PGMEA (484431; Sigma Aldrich) for 3 h at 65 °C. For samples with internal channel structures, 25 mg mL^{-1} EDMAB was added to the post-curing solution to inhibit cationic over-polymerization. Washing in PGMEA for 72 h and in H_2O for another 72 h with solvent-changes twice a day completed the post processing procedure.

Supporting Information

Supporting Information is available from the Wiley Online Library or from the author.

Acknowledgements
Financial support from from Independent Research Fund Denmark, grant 7017-00366B is kindly acknowledged.

Conflict of Interest

The authors declare no conflict of interest.

Received: ((will be filled in by the editorial staff))
Revised: ((will be filled in by the editorial staff))
Published online: ((will be filled in by the editorial staff))

References

[1] N. S. Bhise, J. Ribas, V. Manoharan, Y. S. Zhang, A. Polini, S. Massa, M. R. Dokmeci, A. Khademhosseini, *J. Control. Release* **2014**, *190*, 82.

[2] B. Zhang, A. Korolj, B. F. L. Lai, M. Radisic, *Nat. Rev. Mater.* **2018**, *3*, 257.

[3] H. Liu, Y. Wang, H. Wang, M. Zhao, T. Tao, X. Zhang, J. Qin, *Adv. Sci.* **2020**, *7*, 1903739.

[4] X. Zhang, L. Li, C. Luo, *Lab Chip* **2016**, *16*, 1757.

[5] C. B. Goy, R. E. Chaile, R. E. Madrid, *React. Funct. Polym.* **2019**, *145*, DOI 10.1016/j.reactfunctpolym.2019.104314.

[6] A. K. Au, W. Lee, A. Folch, *Lab Chip* **2014**, *14*, 1294.

[7] R. Amin, S. Knowlton, A. Hart, B. Yenilmez, F. Ghaderinezhad, S. Katebifar, M. Messina, A. Khademhosseini, S. Tasoglu, *Biofabrication* **2016**, *8*, 1.

[8] A. P. Kuo, N. Bhattacharjee, Y. S. Lee, K. Castro, Y. T. Kim, A. Folch, *Adv. Mater. Technol.* **2019**, *4*, 1.

[9] F. Li, N. P. Macdonald, R. M. Guijt, M. C. Breadmore, *Lab Chip* **2019**, *19*, 35.

[10] S. Mi, Z. Du, Y. Xu, W. Sun, *J. Mater. Chem. B* **2018**, *6*, 6191.

[11] A. Dravid, B. Raos, Z. Aqrawe, S. Parittotokkaporn, S. J. O'Carroll, D. Svirskis, *Front. Chem.* **2019**, *7:638*, DOI 10.3389/fchem.2019.00638.

[12] L. Ahrens, S. Tanaka, D. Vonwil, J. Christensen, D. Iber, V. P. Shastri, *Adv. Biosyst.* **2019**, *3*, 1800237.

[13] C. Yang, F. W. DelRio, H. Ma, A. R. Killaars, L. P. Basta, K. A. Kyburz, K. S. Anseth, *Proc. Natl. Acad. Sci.* **2016**, *113*, E4439.

[14] K. C. Hribar, Y. S. Choi, M. Ondeck, A. J. Engler, S. Chen, *Adv. Funct. Mater.* **2014**, *24*, 4922.

[15] X. (James) Li, A. V Valadez, P. Zuo, Z. Nie, *Bioanalysis* **2012**, *4*, 1509.

[16] J. O. Hardin, T. J. Ober, A. D. Valentine, J. A. Lewis, *Adv. Mater.* **2015**, *27*, 3279.

[17] D. Kokkinis, M. Schaffner, A. R. Studart, *Nat. Commun.* **2015**, *6*, 8643.

[18] H. Lee, D. W. Cho, *Lab Chip* **2016**, *16*, 2618.

[19] C. Zhou, Y. Chen, Z. Yang, B. Khoshnevis, *22nd Annu. Int. Solid Free. Fabr. Symp. - An Addit. Manuf. Conf. SFF 2011* **2011**, 65.

[20] X. Wu, Q. Lian, D. Li, Z. Jin, *Rapid Prototyp. J.* **2019**, *25*, 277.

[21] J. W. Choi, H. C. Kim, R. Wicker, *J. Mater. Process. Technol.* **2011**, *211*, 318.

[22] D. Han, C. Yang, N. X. Fang, H. Lee, *Addit. Manuf.* **2019**, *27*, 606.

[23] A. K. Miri, D. Nieto, L. Iglesias, H. Goodarzi Hosseinabadi, S. Maharjan, G. U. Ruiz-Esparza, P. Khoshakhlagh, A. Manbachi, M. R. Dokmeci, S. Chen, S. R. Shin, Y. S. Zhang, A. Khademhosseini, *Adv. Mater.* **2018**, *30*, 1800242.

[24] G. I. Peterson, J. J. Schwartz, D. Zhang, B. M. Weiss, M. A. Ganter, D. W. Storti, A. J. Boydston, *ACS Appl. Mater. Interfaces* **2016**, *8*, 29037.

[25] A. Muralidharan, A. C. Uzcategui, R. R. McLeod, S. J. Bryant, *Adv. Mater. Technol.* **2019**, *4*, 1900592.

[26] X. Kuang, J. Wu, K. Chen, Z. Zhao, Z. Ding, F. Hu, D. Fang, H. J. Qi, *Sci. Adv.* **2019**, *5*, eaav5790.

[27] W. Li, M. Bakhtiary Noodeh, N. Delpouve, J. M. Saiter, L. Tan, M. Negahban, *Express Polym. Lett.* **2016**, *10*, 1003.

[28] N. D. Dolinski, Z. A. Page, E. B. Callaway, F. Eisenreich, R. V. Garcia, R. Chavez, D. P. Bothman, S. Hecht, F. W. Zok, C. J. Hawker, *Adv. Mater.* **2018**, *30*, 1800364.

[29] J. J. Schwartz, A. J. Boydston, *Nat. Commun.* **2019**, *10*, 791.

[30] E. K. U. Larsen, N. B. Larsen, K. Almdal, *J. Polym. Sci. Part B Polym. Phys.* **2016**, *54*, 1195.

[31] J. V. Crivello, *J. Polym. Sci., Part A: Polym. Chem.* **1999**, *37*, 4241.

[32] J. V. Crivello, S. Rajaraman, W. A. Mowers, S. Liu, *Macromol. Symp.* **2000**, *157*, 109.

[33] X. Ge, Q. Ye, L. Song, A. Misra, P. Spencer, *RSC Adv.* **2015**, *5*, 77791.

[34] M. Sangermano, *J. Photopolym. Sci. Technol.* **2019**, *32*, 233.

[35] L. F. J. Schneider, L. M. Cavalcante, S. Consani, J. L. Ferracane, *Dent. Mater.* **2009**, *25*, 369.

[36] P. F. Jacobs, *Soc. Manuf. Eng.* **1992**, 196.

[37] C. Hofstetter, S. Orman, S. Baudis, J. Stampfl, *Addit. Manuf.* **2018**, *24*, 166.

[38] A. C. Uzcategui, A. Muralidharan, V. L. Ferguson, S. J. Bryant, R. R. McLeod, *Adv. Eng. Mater.* **2018**, *20*, 1800876.

[39] H. Gong, M. Beauchamp, S. Perry, A. T. Woolley, G. P. Nordin, *RSC Adv.* **2015**, *5*, 106621.

[40] F. Wang, O. Sigmund, J. S. Jensen, *J. Mech. Phys. Solids* **2014**, *69*, 156.

[41] D. Van Swaay, J. P. Mächler, C. Stanley, A. Demello, *Lab Chip* **2014**, *14*, 178.

[42] R. Zhang, N. B. Larsen, *Lab Chip* **2017**, *17*, 4273.

[43] N. K. Singha, B. de Ruiter, U. S. Schubert, *Macromolecules* **2005**, *38*, 3596.

A dual material stereolithographic 3D printing method based on orthogonal radical or cationic photopolymerization is presented. Two distinct materials can be locally polymerized in parallel, controlled by the illumination wavelength. The method is demonstrated by combining a diffusion-open PEGDA hydrogel and a tough, interpenetrating PEGDA/epoxy material at high resolutions to create complex monolithic devices, of use in advanced cell culture.

Stereolithography

C. Schmidleithner, R. Zhang, N. Taebnia, E. K. U. Larsen, K. Almdal, N. B. Larsen*

High Resolution Dual Material Stereolithography for Monolithic Microdevices